Vortex-induced dispersal of a plant pathogen by raindrop impact

Seungho Kim[a], Hyunggon Park[b], Hope A. Gruszewski[c], David G. Schmale III[c], and Sunghwan Jung[a,1]

[a]Department of Biological and Environmental Engineering, Cornell University, Ithaca, NY 14853; [b]Department of Biomedical Engineering and Mechanics, Virginia Polytechnic Institute and State University, Blacksburg, VA 24061; and [c]School of Plant and Environmental Sciences, Virginia Polytechnic Institute and State University, Blacksburg, VA 24061

Edited by David A. Weitz, Harvard University, Cambridge, MA, and approved January 15, 2019 (received for review November 28, 2018)

Raindrop impact on infected plants can disperse micron-sized propagules of plant pathogens (e.g., spores of fungi). Little is known about the mechanism of how plant pathogens are liberated and transported due to raindrop impact. We used high-speed photography to observe thousands of dry-dispersed spores of the rust fungus *Puccinia triticina* being liberated from infected wheat plants following the impact of a single raindrop. We revealed that an air vortex ring was formed during the raindrop impact and carried the dry-dispersed spores away from the surface of the host plant. The maximum height and travel distance of the airborne spores increased with the aid of the air vortex. This unique mechanism of vortex-induced dispersal dynamics was characterized to predict trajectories of spores. Finally, we found that the spores transported by the air vortex can reach beyond the laminar boundary layer of leaves, which would enable the long-distance transport of plant pathogens through the atmosphere.

plant pathogen | dry rust spore | air vortex | swirling trajectory | drop impact

Plant diseases threaten our food safety and security (1, 2). Some plant pathogens can be spread by rainfall (3–6), in which splashing droplets carry pathogenic spores within and among susceptible host plants (3). Small splashing droplets with a diameter of <100 μm can be carried via wind currents (7, 8). However, most satellite droplets from drop impacts are larger than 100 μm (3) and are too heavy to follow wind flows over long distances, typically less than a few tens of centimeters (4, 5).

Previous studies have shown that plant pathogens such as rusts can be transported kilometer distances in the atmosphere (9) and even cross continents (10–13). In 1963, Hirst and Stedman (14) showed an increase in the concentration of dry-dispersed rust spores in the atmosphere followed by raindrop impacts. Other bioaerosols have been observed to increase shortly after rainfall (15) and then stay up in the air for several hours (16). Once airborne, these small dry-dispersed spores can avoid the scavenging of raindrops by following air streamlines around the falling raindrops, while large particles are scavenged by raindrops (17, 18). New information is needed on the liberation mechanism of spores from infected plants, and how these spores might be transported over long distances.

In this present work, we observed the liberation of dry-dispersed spores following simulated raindrop impacts on wheat leaves infected with the rust fungus *Puccinia triticina*. In addition, glass particles similar to the rust spores in size were used for a parametric study and to visualize dry spreading mechanisms at a greater level of detail. We describe and explain how an air vortex is formed after a drop impacts the leaf surface and carries dry-dispersed (not wetted by a raindrop) spores away from the plant surface. Consequently, dry spores dispersed by the air vortex induced by drop impact have the potential to traverse the laminar boundary layer and travel over longer distances (19). The mechanism of the air-vortex dispersal could explain abrupt increases in dry-dispersed spores in the atmosphere immediately after rainfall events and also the transport of plant pathogens over long distances.

Results

Types of Spore Dispersal. We observed and analyzed the dispersal motion of urediniospores of *P. triticina* when a raindrop hits an infected leaf containing uredinia (Fig. 1*A*). Fig. 1*B* shows that a falling drop is powerful enough to liberate spores. Here, we identified two types of spore dispersal. The first is a wet splash dispersal of spores that has been studied previously. When a droplet impacts a surface, the contact line of the spreading edge of the drop becomes unstable and forms several daughter splash droplets due to the high inertia of the drop and the hydrophobic property of a leaf substrate (20). As shown on the right side of Fig. 1*B*, splashing droplets fly out along with spores inside. Spores inside a splash droplet are shown in Fig. 1*C* and *SI Appendix*, section A. Although the number of spores inside a splash droplet is more than that of dry-dispersed spores (5), the splash droplets are too heavy to follow the surrounding air current, limiting the range of dispersal.

The second is a dry-spore dispersal, that is, not wetted by a raindrop. The dry-spore dispersal is attributed to either the vibration of a wheat leaf (Fig. 1*B*) or the direct impact of the drop (Fig. 1*C*, *Inset*). Most spores are liberated from the upper surface, especially due to drop impact (top right side of Fig. 1*B*). However, spores on the lower surface can be thrown by a rapidly decelerating leaf, but the number of ejected spores from the lower surface is less than that from the upper surface.

Measurement of the Number of Ejected Spores. We measured the number of dry-dispersed spores, N_s, after a drop impact. We first attached a rust-infected wheat leaf on a Petri dish. Then, a drop was released onto the wheat leaf at different heights to vary the

Significance

Understanding the spread of spores of plant pathogens, some of which may serve as potential human allergens, is of great importance to plant and animal health. Raindrop impact is known to be a mechanism for dispersing micron-sized pathogenic spores. However, previous studies have focused only on wet splash droplets formed by raindrop impact, which our results suggest are only a minor contributor to spore dispersal. Our experiments show the importance of air vortices resulting from the drop impacts to disperse spores beyond the laminar boundary layer, with the potential for transport over long distances.

Author contributions: S.K., H.P., H.A.G., and S.J. designed research; S.K., H.P., and S.J. performed research; S.K., H.P., D.G.S., and S.J. analyzed data; and S.K., H.P., H.A.G., D.G.S., and S.J. wrote the paper.

The authors declare no conflicts of interest.

This article is a PNAS Direct Submission.

[1]To whom correspondence should be addressed. Email: sunnyjsh@cornell.edu.

This article contains supporting information online at www.pnas.org/lookup/suppl/doi:10.1073/pnas.1820318116/-/DCSupplemental.

Published online February 25, 2019.

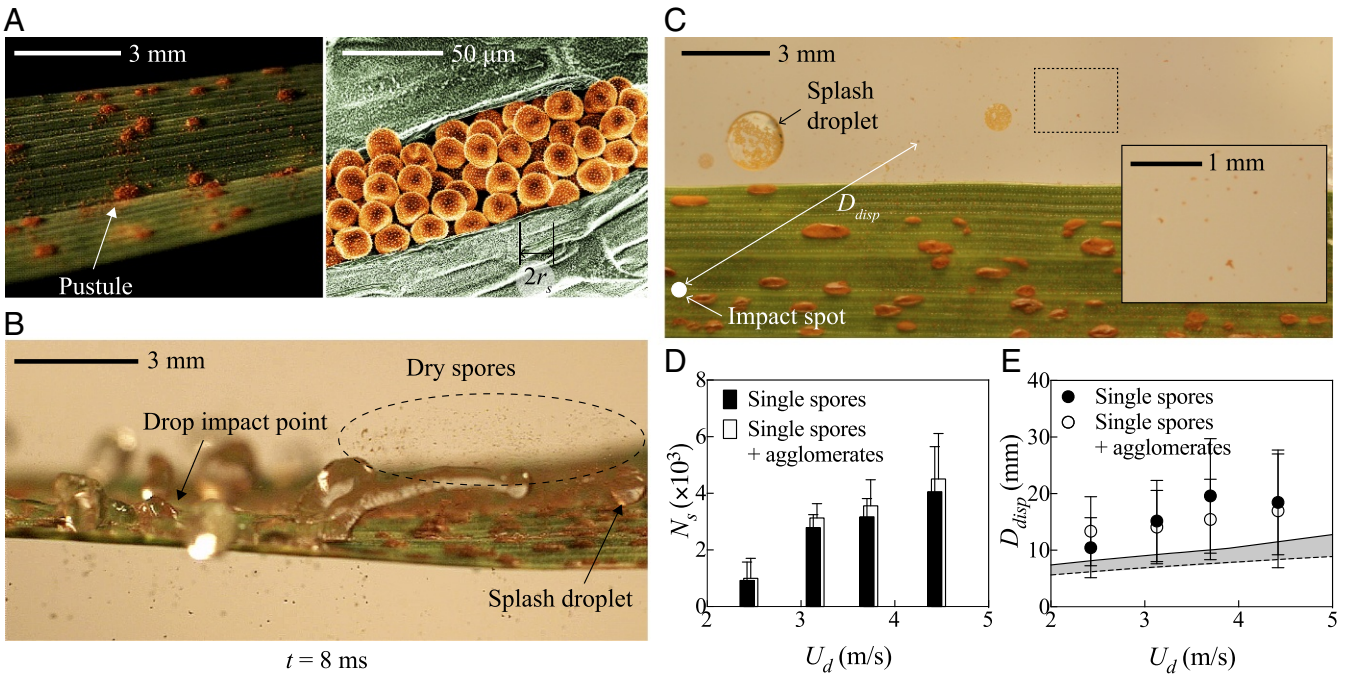

Fig. 1. (*A*) Rust-infected wheat leaf surface (*Left*) and SEM image of a uredinium (rust pustule containing urediniospores) (*Right*). Here, a pustule of spores is seen on the epidermis of the wheat leaf. (*B*) Dispersal of thousands of dry spores by drop impact when $[R_d, U_d] = [1.6$ mm, 2.4 m/s$]$, where R_d, U_d are the radius and velocity of the impacting drop, respectively. (*C*) Visualization of dispersal patterns at $[R_d, U_d] = [1.8$ mm, 2.8 m/s$]$. (*Inset*) Dry-dispersed spores discharged by drop impact. (*D*) The number N_s and (*E*) dispersal distance D_{disp} of dry spores versus impact velocity U_d for a drop of 1.8-mm radius. The gray area in *E* corresponds to the calculated distance of dispersed spores without an air vortex. The filled bars and circles are for single spores only, whereas the open bars and circles are for all spores including spore agglomerates (more than one spore).

impact speed. We measured the number of dry-dispersed spores using a Nikon D500 camera with a pixel resolution of 6,016 × 4,000; the area of most spores was measured to be about five square pixels (*SI Appendix*, section A). Fig. 1*C* shows both wet-dispersed spores and thousands of dry-dispersed spores. Fig. 1*D* shows that the number of dry-dispersed spores, N_s, is on the order of 10^3 and increases with the impact velocity, U_d. Such an increase of N_s with respect to U_d can be attributed not only to higher impulse momentum (5) but also to an increase in the drop-contact area as the drop spreads (21).

Ejection Mechanism. Spores are detached by the spreading motion of a drop as it exerts dynamic force on the spores. The dynamic force to drag and scavenge spores, $C_D \rho_d U_c^2 r_s^2$ (~ 10 nN), exceeds the interparticle force of *P. triticina* spores, 0.7 nN (*SI Appendix*, section B). Here, C_D, ρ_d, U_c, and r_s are the drag coefficient, the liquid density, the speed of the liquid contact line (on the order of 1 m/s), and the radius of a spore (≈ 10 μm). The detached spores stay on the advancing meniscus and then collide with dry spores on the way. By assuming elastic collision between spores on the meniscus and dry spores, the ejection velocity of dry spores, V_e, would be proportional to the impact velocity of a falling drop, U_d. A detailed theoretical model and experimental validation of spore ejection are presented in *SI Appendix*, section C.

Spore-Traveling Distance and Trajectory. For spores moving through quiescent air, the Reynolds number, $Re_s = \rho_a V_s (2r_s)/\mu_a \lesssim 1$, is small, where ρ_a and μ_a are the density and dynamic viscosity of air ($\rho_a = 1.2$ kg/m^3, $\mu_a = 1.82 \times 10^{-5}$ Pa·s), and V_s is the instantaneous speed of a spore. Here, the instantaneous speed decreases over time due to the air drag after reaching its maximum speed at the moment of ejection ($V_e \sim 1$ m/s). Thus, the trajectory of spores can be predicted by balancing inertial force $\rho_s (4/3)\pi r_s^3 (d\vec{V}_s/dt)$, Stokes drag $6\pi\mu_a \vec{V}_s r_s$, and gravity, where ρ_s is the spore density. By integrating these forces with the initial condition as $V_s(t=0) = V_e$, a spore-travel distance d_{trav} can be written as follows:

$$d_{trav} = \frac{2\rho_s r_s^2 V_e \cos\alpha_e}{9\mu_a}\left[1 - e^{-9\mu_a t_r/(2\rho_s r_s^2)}\right], \qquad [1]$$

where α_e and t_r correspond to the ejection angle and residence time of a spore in air, respectively. For ejected spores with $V_e = 1$ m/s, the relaxation timescale, $\tau_s = (2/9)\rho_s r_s^2/\mu_a$, is about 10^{-3} s, whereas the residence timescale, t_r, becomes only 10^{-2} s. Therefore, the travel distance, d_{trav}, is close to $V_e \tau_s \cos\alpha_e$ since the exponential term, e^{-t_r/τ_s}, in Eq. **1** is quite small, on the order of 10^{-5}.

Fig. 1*C* shows horizontal distances of dispersed spores measured from the drop-impact point, D_{disp}. To avoid any confusion, it is worth mentioning that the travel distance, d_{trav}, is measured from spore's resting position, not from the drop-impact point. Hence, d_{trav} is always smaller than D_{disp}. Interestingly, we found that the dispersal distance of spores exceeds theoretical values from the above force balance. Fig. 1*E* shows the consistent discrepancy over different drop speeds.

To rectify the discrepancy on dispersal distance, we visualized the side-view trajectory of rust spores as in Fig. 2*A*, which shows that spores ballistically move shortly after the ejection (see the upper panel inset) and then swirl around (see the lower panel inset). The overall trajectory of one spore is shown as the black line in the lower panel. Fig. 2*B* illustrates a detailed trajectory from an experiment and a simulated trajectory using the ballistic model above. The ballistic model shows a right-triangle path (closed symbols) known as the Tartaglia's trajectory (22), whereas the experimental trajectory presents a swirling motion with a longer travel distance (open symbols). In addition, the maximum height reached by the spore is a bit higher than the predicted height from the ballistic model. To explain this

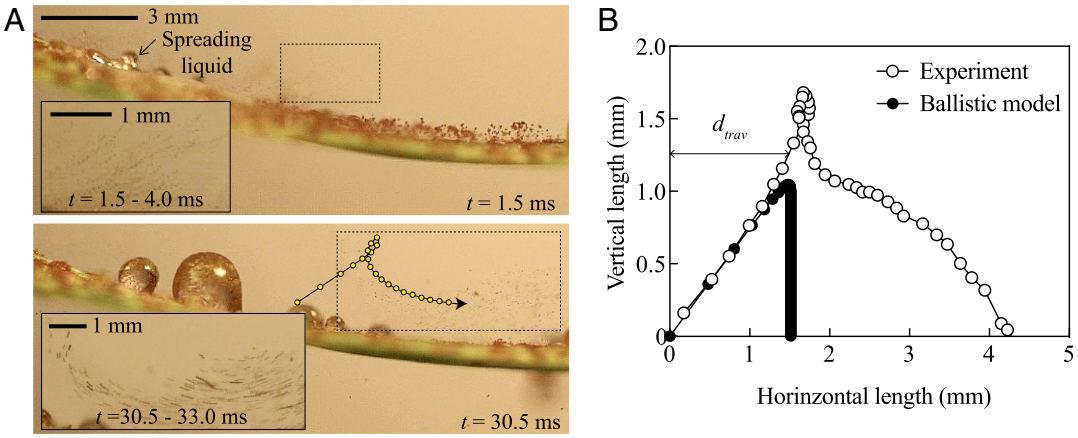

Fig. 2. (*A*) Visualization of spores of *P. triticina* motions moving around a wheat leaf when a raindrop of $[R_d, U_d] = [1.6$ mm, 2.4 m/s] impacts the leaf surface. Dry-dispersed wheat spores escape from the leaf, showing swirling trajectories during their dispersal (a solid curve with circles is obtained by tracking one spore). Each inset shows overlapping multiple images to visualize the trajectories of dry-dispersed spores (Movies S1 and S2). (*B*) Comparison of spore trajectories obtained from an experiment and from a ballistic model.

discrepancy, we need to understand airflow around liberated spores upon drop impact.

Trajectory Comparison Using Artificial Spores. To visualize the airflow, we used glass beads as surrogates for spores (glass sphere type I in Table 1). The density and radius of particles are close to those of actual wheat spores. We observed similar dispersal behaviors of actual wheat spores. In the very beginning, ballistic trajectories were observed as shown in the first panel of Fig. 3. Then, the glass beads were swirling around and slowly move to the right (the second, third, and fourth panels of Fig. 3). Since the glass beads are light, this swirling motion can represent the pathlines of air current. To confirm this, we calculated the Stokes number, St, defined as a ratio of the relaxation time of a particle τ_s $(=2/9\rho_s r_s^2/\mu_a)$ to the characteristic flow time τ_f $(=\bar{r}_w/\bar{U}_w)$. Here $\bar{r}_w \sim 1$ mm and $\bar{U}_w \sim 0.1$ m/s are the mean radius and velocity of the swirling flows. The Stokes number is very small for artificial spore I ($St = 0.001 - 0.13$). Also, for the wheat spore, St is also 0.15, which indicates that such swirling motion is induced by surrounding airflows.

Effect of Surrounding Airflows. Bischofberger et al. (23) showed the experimental evidence of a vortex ring created by a spreading drop. Here, we also visualized the vortex ring using a smoke generator (Chauvet DJ H700), as shown in Fig. 4*A*. Fig. 4*B* shows the schematic of forming the air vortex via a spreading drop. The airflow was induced by the spreading drop, whose speed was proportional to the inertia of the impacting drop. Then, a vortex ring was shed as a boundary layer keeps propagating laterally, after the spreading drop reached its maximum radius. We experimentally measured the initial magnitude of circulation using particle tracking velocimetry (PTV) (*SI Appendix*, section D). Fig. 4*C* shows that $\Gamma(t \approx 0)$ is proportional to U_d and R_d, which indicates that circulation $\Gamma(t \approx 0)$ was induced by the drop inertia. Also, we observed that the air vortex is dissipated over time and lasted only for a few tens of milliseconds, as shown in Fig. 4*E*. Therefore, airborne spores are swirled up by an air vortex and then fall back under gravity after a few tens of milliseconds, which can explain complicated trajectories in Fig. 2.

Theoretical Model of the Magnitude of Circulation in Air. We developed a scaling relation of $\Gamma(t \approx 0)$ for a better understanding of the vortex motion. The shear motion of a spreading drop drives airflow and eventually creates an air vortex in the air. This spreading energy per unit length, E_D, is given as $\int_0^{t_m}\int_\Omega \phi \, d\Omega dt \approx \phi \Omega t_m$, where ϕ, Ω, and t_m are the viscous dissipation function per unit length, the effective area of a viscous fluid, and the time duration for a spreading drop to reach its maximum radius, respectively. The dissipation function ϕ scales as $\mu_a(\bar{U}_c/\delta_a)^2 \sim \mu_a \bar{U}_c^2/(R_d^2 Re_a^{-1})$ using the Blasius boundary thickness of air, δ_a, where $\bar{U}_c$ and Re_a are the mean speed of a liquid contact line and the Reynolds number of air, $\rho_a U_d(2R_d)/\mu_a$. The cross-sectional area of the boundary layer scales as $\Omega \sim R_m \delta_a$ and $t_m \sim R_d/U_d$. Also, the maximum spreading radius of an impacting drop, R_m, scales as $R_d Re_d^{1/4}$ (21), where $Re_d = \rho_d U_d(2R_d)/\mu_d$ with the dynamic viscosity of a liquid, μ_d. We finally get the spreading energy as $E_D \sim \mu_a R_d U_d Re_a^{1/2} Re_d^{3/4}$ by substituting R_m and $\bar{U}_c$ as derived in *SI Appendix*, section E. The rotational energy of the air vortex, E_R, is given as $\rho_a \Gamma^2(t \approx 0) = \rho_a \bar{r}_w^2(\bar{r}_w \bar{w})^2$ (24), where $\bar{r}_w$ and $\bar{w}$ are the mean radius and vorticity of the air vortex, respectively. By balancing spreading and rotational energies, we get the circulation as

$$\Gamma(t \approx 0) \sim Re_a^{-1/4} Re_d^{3/8} U_d R_d. \quad [2]$$

Our scaling relation shows the dependence of Re_a on the initial circulation, $\Gamma(t \approx 0)$. Fig. 4*D* shows good agreement of our scaling argument with experimental data. Furthermore, this association explains experimental observations previously reported in ref. 23.

Simulation of Spore Trajectories. We also simulated the trajectories of spores by solving the equation of motion considering inertial force, air drag force, and gravitational force:

$$\rho_s \left(\frac{4}{3}\pi r_s^3\right) \frac{d\vec{V}_s}{dt} = 6\pi\mu_a r_s(\vec{V}_s - \vec{U}_w) - \rho_s \left(\frac{4}{3}\pi r_s^3\right)\vec{g}. \quad [3]$$

Here, $\vec{g}$ is the gravitational acceleration and we neglect the Basset force because of low ρ_a and μ_a. To estimate the airflow, $\vec{U}_w$, we used potential theory and the method of images along with our estimated circulation. Thus, the corresponding

Table 1. Properties of artificial spores

Type	Particle	ρ_s, kg/m^3	r_s, μm
I	Hollow glass sphere	1,100	1 to 10
II	Soda lime sphere	2,500	19.0 to 22.5
III	Soda lime sphere	2,500	45.0 to 53.0

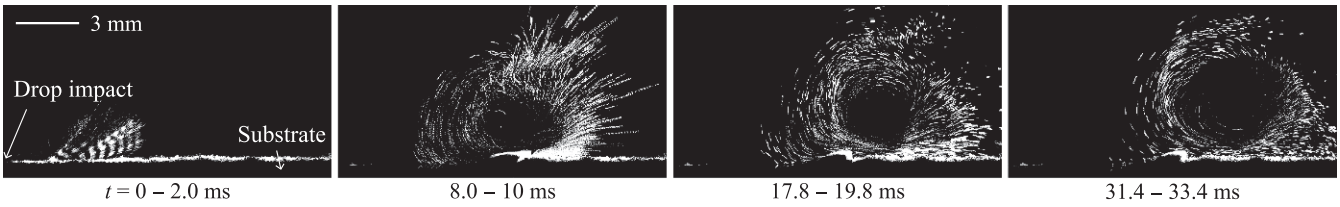

Fig. 3. Visualization of the dispersal motion of glass beads (surrogates for spores) when [R_d, U_d] = [1.9 mm, 3.1 m/s]. Ballistic motion of the beads was observed only at the beginning stage of dispersal, but later spores exhibited a swirling motion (Movies S3 and S4).

complex potential W can be written as $W = -i\Gamma/(2\pi) \log[(z-d)/(z+d)]$ (25), where z is a complex variable of a position and d is a distance from the wall. Here, the vortex circulation, Γ, dissipates over time after the vortex is shed from a spreading drop. The wall distance, d, increases over time as $d \sim \sqrt{\nu_a t}$, where ν_a is the kinematic viscosity of air while the vortex dissipates and diffuses away (*SI Appendix*, section F). By differentiating W with respect to z, we can determine $\vec{U}_w$. Finally, we can numerically solve Eq. **3** with given ejection velocity and angle of spores. Fig. 5 shows that computed trajectories from Eq. **3** follow experimental trajectories quite well.

The vortex generated from a spreading raindrop can blow spores farther away and also cause the swirling motion of the spores, resulting in transport over higher and longer distances. Fig. 5 also shows that the maximum height of liberated spores increases in the presence of the air vortex (red and orange circles and lines), and thus most liberated spores can escape beyond the boundary layer of a leaf ($\delta_L \approx 1.72\sqrt{\nu_a L/U} \approx 0.7 - 2.1$ mm; the length of leaf, $L \approx 10$ cm; and a typical wind speed, $U = 1 - 10$ m/s) (26). Thus, spores liberated by an air vortex may cross the laminar boundary layer and be exposed to the wind, with the potential to travel over long distances in the atmosphere.

Discussion

Various spore-dispersal mechanisms have been reported previously. These include dispersal resulting from changes in temperature and relative humidity (27), in response to mechanical stimuli (28), from insect movement (29), along with dew and splash droplets (30), and due to cavitation bubbles (31). In this paper, we report a dry-dispersal mechanism of a plant pathogen via raindrop impact. When a raindrop hits a rust-infected plant leaf, the drop initially pushes the spores to be liberated from the leaf surface. Then, the spores follow swirling trajectories aided by the air vortex ring formed by the raindrop. As a result, the spores travel longer distances and reach greater heights, thereby reaching outside the boundary layer to be swept away by wind. Therefore, a number of pathogenic spores can escape

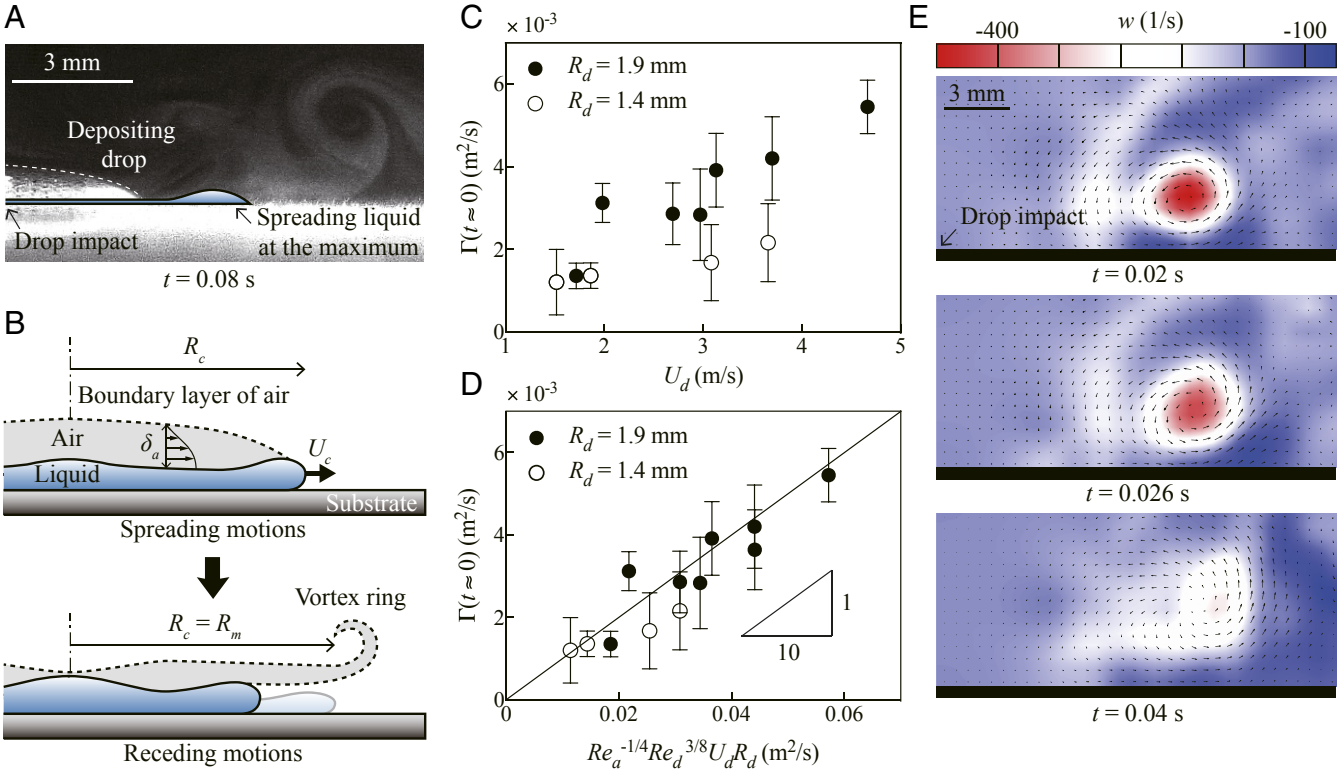

Fig. 4. (*A*) Smoke visualization of the air vortex with [R_d, U_d] = [1.4 mm, 3.3 m/s]. The white dashed curve represents the final shape of a drop and the solid curve indicates the intermediate shape of a spreading drop at the maximum spreading radius. (*B*) Schematic of the formation of an air vortex, driving spores to swirl around. (*C*) Magnitude of a circulation Γ versus an impact velocity U_d depending on a drop radius R_d. (*D*) Γ is replotted according to our scaling law (Eq. **2**). (*E*) Contour map of a vorticity obtained from particle image velocimetry (PIV) measurements using glass beads with [R_d, U_d] = [1.9 mm, 3.1 m/s], showing the dissipation of the air vortex with elapsed times (see *SI Appendix*, section D).

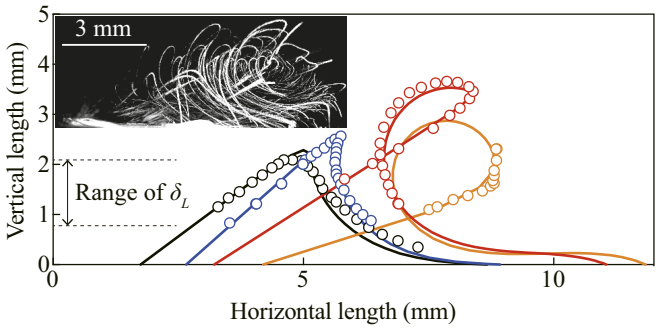

Fig. 5. Experimental (circles) and theoretical (solid lines) footprints of glass beads, where [R_d, U_d] = [1.4 mm, 3.2 m/s]. (*Inset*) The actual trajectories of glass beads I, obtained from overlapping multiple images from t = 0.4 to 76 ms.

from the region of an infected plant and possibly land on other susceptible plants.

A few limitations exist to simulating the trajectory of rust spores: splash droplets and the leaf's flexibility. First, the splash droplets affect the shape and magnitude of the air vortex, which change the trajectory of spores only near the end (*SI Appendix*, section F). Second, a flexible leaf will vibrate due to the drop impact, which increases the number of spores. However, the response of the leaf is much longer than spreading time of the drop, which minimizes its effect on liberated spores. Nevertheless, we consistently observed that both rust spores and surrogate glass beads show the swirling trajectories (Fig. 2) and are able to escape from the leaf boundary as d_{trav} and maximum height are larger than the width of leaf and δ_L, respectively. Our finding could be extended to crops impacted by rust diseases, such as coffee and corn, thereby making d_{trav} much longer than that without the air vortex (*SI Appendix*, section G).

Outside the boundary layer, air flows are turbulent. So, the Stokes number of spores in that region is much less than 1; $St_k = \tau_s/\tau_k$ where the particle relaxation timescale is $\tau_s = (2/9)\rho_s r_s^2/\mu_a \sim 10^{-3}$ s and the Kolmogorov timescale is $\tau_k = (\nu_a/\epsilon)^{1/2} = 10^{-2} - 10^{-1}$ s. The turbulent kinetic dissipation rate ϵ is expected to be $10^{-3} - 10^{-2}$ m^2/s^3 at the half-height of a typical canopy (32). Thus, many airborne spores with $St_k < 1$ can be immediately dispersed by the turbulent eddies, similar to ocean spray droplets (33). Furthermore, plant pathogens can travel over kilometer distances via wind currents (34). Therefore, the dry dispersal of plant pathogens via a vortex ring may be a critical component of the spread of a plant pathogen in the atmosphere over long distances in the atmosphere.

Materials and Methods

Preparation of Infected Wheat Leaves. Lines of wheat susceptible to wheat leaf rust infection were cultivated under controlled growth conditions (135 μmol·m^{-2}·s^{-1} light for 12 h/d, 25°C) for 6 wk following seed germination. Healthy leaves were inoculated using a suspension of *P. triticina* urediniospores in water with 0.001% of detergent as an adjuvant. Inoculated plants were then incubated in an isothermal–isohumidity chamber at 15°C and 99% relative humidity for 24 h then removed back to previous controlled growth conditions. After 7 to 10 d, pustules of *P. triticina* spores had sufficiently broken through the epidermis of wheat leaf, as illustrated in Fig. 1*A*.

Properties of Rust Pustules and Spores. The shape of the pustules is assumed to be an elliptic cylinder, where the length of major and minor axes were measured to be 1.02 ± 0.17 mm and 0.30 ± 0.04 mm, respectively, and the thickness is measured to be 0.21 ± 0.01 mm. The radius of *P. triticina* spores, r_s, was measured to be 9.7 ± 0.6 μm using a scanning electron microscope. Measuring the terminal velocity of individually falling spores, the density of *P. triticina* spores, ρ_s, was calculated to be 1,294 ± 84 kg/m^3 (*SI Appendix*, section H), whose value is close to the density of other microspores, such as fungal spores (35) and pollen (36).

Drop Impact Conditions. A syringe needle was used to generate water drops of radius R_d ranging from 1.4 to 1.9 mm, within the range of the typical size of raindrops (37). Drops were released from a certain height, falling under gravity, and then striking either an anchored leaf (cantilever) or a leaf fully supported by a rigid bottom. By varying the drop-releasing height from the substrate, the impact velocity of a water drop, U_d, is changed to be between 1.5 and 4.6 m/s. Thus, the corresponding Weber $We_d = \rho_d U_d^2(2R_d)/\gamma$ and Reynolds number $Re_d = \rho_d U_d(2R_d)/\mu_d$ of an impacting drop range from 88 to 1,117 and from 4,200 to 17,480, respectively. Here we specially focused on drop impact on a rigid infected leaf to elucidate the fundamental mechanisms of vortex-induced spore spreading. In the timescale comparison, the spreading time of water drops, $t_m \sim R_d/U_d$, is on the order of 1 ms, which is much less than the vibration time of leaves [~50 ms (38)]. Thus, the vibration of the leaf by drop impact is assumed to be insignificant to the initial liberation process of disease spreading. Also, we focused on the first impact of a simulated raindrop because the number of the removed spores was observed to rapidly decrease with the number of successive drop impacts (5).

Properties of Artificial Leaf and Spores. Artificial leaf and spores were used to quantify the dynamics of disease spreading. For the artificial leaf, we used a polycarbonate film. For the artificial spores, we used micron-sized glass beads listed in Table 1. When the glass beads were disposed onto a substrate, the thickness ranged between 100 and 250 μm, which is a value similar to the thickness of pustules. Here, the Stokes numbers of artificial spores I, II, and III were measured to be 0.001 to 0.13, 1.1 to 1.5, and 6.1 to 8.5, respectively.

ACKNOWLEDGMENTS. We thank Todd Gidley for initial contributions. This work was supported by National Science Foundation Grant CBET-1604424 and US Department of Agriculture Grant 2018-67013-28063.

1. Strange RN, Scott PR (2005) Plant disease: A threat to global food security. *Annu Rev Phytopathol* 43:83–116.
2. Park RF (2007) Stem rust of wheat in Australia. *Aust J Agric Res* 58:558–566.
3. Gilet T, Bourouiba L (2015) Fluid fragmentation shapes rain-induced foliar disease transmission. *J R Soc Interface* 12:20141092.
4. Cevallos-Cevallos JM, Danyluk MD, Gu G, Vallad GE, Van Bruggen AHC (2012) Dispersal of salmonella typhimurium by rain splash onto tomato plants. *J Food Prot* 75:472–479.
5. Geagea L, Huber L, Sache I (1999) Dry-dispersal and rain-splash of brown (Puccinia recondita f. sp. tritici) and yellow (p. striiformis) rust spores from infected wheat leaves exposed to simulated raindrops. *Plant Pathol* 48:472–482.
6. Yang X, Madden LV, Reichard DL, Fox RD, Ellis MA (1991) Motion analysis of drop impaction on a strawberry surface. *Agric For Meteorol* 56:67–92.
7. Hobson PA, Miller PCH, Walklate PJ, Tuck CR, Western NM (1993) Spray drift from hydraulic spray nozzles: The use of a computer simulation model to examine factors influencing drift. *J Agric Eng Res* 54:293–305.
8. Miller P (2003) The measurement of spray drift. *Pestic Outlook* 14:205–209.
9. Hirst JM, Stedman OJ, Hogg WH (1967) Long-distance spore transport: Methods of measurement, vertical spore profiles and the detection of immigrant spores. *J Gen Microbiol* 48:329–355.
10. Brown JKM, Hovmøller MS (2002) Aerial dispersal of pathogens on the global and continental scales and its impact on plant disease. *Science* 297:537–541.
11. Aylor DE (2003) Spread of plant disease on a continental scale: Role of aerial dispersal of pathogens. *Ecology* 84:1989–1997.
12. Hovmøller MS, Yahyaoui AH, Milus EA, Justesen AF (2008) Rapid global spread of two aggressive strains of a wheat rust fungus. *Mol Ecol* 17:3818–3826.
13. Nagarajan S, Singh DV (1990) Long-distance dispersion of rust pathogens. *Annu Rev Phytopathol* 28:139–153.
14. Hirst JM, Stedman OJ (1963) Dry liberation of fungus spores by raindrops. *J Gen Microbiol* 33:335–344.
15. Cevallos-Cevallos JM, Gu G, Danyluk MD, Dufault NS, van Bruggen AHC (2012) Salmonella can reach tomato fruits on plants exposed to aerosols formed by rain. *Int J Food Microbiol* 158:140–146.
16. Huffman JA, et al. (2013) High concentrations of biological aerosol particles and ice nuclei during and after rain. *Atmos Chem Phys* 13:6151–6164.
17. Chate DM, Pranesha TS (2004) Field studies of scavenging of aerosols by rain events. *J Aerosol Sci* 35:695–706.
18. Mircea M, Stefan S, Fuzzi S (2000) Precipitation scavenging coefficient: Influence of measured aerosol and raindrop size distributions. *Atmos Environ* 34:5169–5174.
19. Schmale DG, III, Ross SD (2015) Highways in the sky: Scales of atmospheric transport of plant pathogens. *Annu Rev Phytopathol* 53:591–611.
20. Josserand C, Thoroddsen ST (2016) Drop impact on a solid surface. *Annu Rev Fluid Mech* 48:365–391.

21. Pasandideh-Fard M, Qiao YM, Chandra S, Mostaghimi J (1996) Capillary effects during droplet impact on a solid surface. *Phys Fluids* 8:650–659.
22. Tartaglia N (1984) *La Nova Scientia* (A. Forni Editore, Bologna, Italy).
23. Bischofberger I, Ray B, Morris JF, Lee T, Nagel SR (2016) Airflows generated by an impacting drop. *Soft Matter* 12:3013–3020.
24. Kim H, Lee J, Kim T-H, Kim H-Y (2015) Spontaneous marangoni mixing of miscible liquids at a liquid–liquid–air contact line. *Langmuir* 31:8726–8731.
25. Acheson DJ (1990) *Elementary Fluid Dynamics*, Oxford Applied Mathematics and Computing Science Series (Clarendon, Oxford).
26. Batchelor GK (1967) *An Introduction to Fluid Dynamics*, Cambridge Mathematical Library (Cambridge Univ Press, Cambridge, UK).
27. Hildebrand PD (2002) Dispersal of plant pathogens. *Encyclopedia of Pest Management* (Dekker, New York), pp 193–196.
28. Gregory PH (1949) The operation of the puff-ball mechanism of lycoperdon perlatum by raindrops shown by ultra-high-speed schlieren cinematography. *Trans Br Mycol Soc* 32:11–15.
29. Ingold CT (1971) *Fungal Spores: Their Liberation and Dispersal* (Clarendon, Oxford).
30. Hirst JM (1953) Changes in atmospheric spore content: Diurnal periodicity and the effects of weather. *Trans Br Mycol Soc* 36:375–393.
31. Noblin X, et al. (2012) The fern sporangium: A unique catapult. *Science* 335: 1322.
32. Poggi D, Katul GG (2010) Evaluation of the turbulent kinetic energy dissipation rate inside canopies by zero- and level-crossing density methods. *Boundary Layer Meteorol* 136:219–233.
33. Veron F (2015) Ocean spray. *Annu Rev Fluid Mech* 47:507–538.
34. Norros V, et al. (2014) Do small spores disperse further than large spores? *Ecology* 95:1612–1621.
35. Roper M, et al. (2010) Dispersal of fungal spores on a cooperatively generated wind. *Proc Natl Acad Sci USA* 107:17474–17479.
36. Jackson ST, Lyford ME (1999) Pollen dispersal models in quaternary plant ecology: Assumptions, parameters, and prescriptions. *Bot Rev* 65:39–75.
37. Laws JO, Parsons DA (1943) The relation of raindrop-size to intensity. *Trans Am Geophys Union* 24:452–460.
38. Gart S, Mates JE, Megaridis CM, Jung S (2015) Droplet impacting a cantilever: A leaf-raindrop system. *Phys Rev Appl* 3:044019.